Sinusoidal voltage protocols for rapid characterization of ion channel kinetics

Kylie A. Beattie[1,2], Adam P. Hill[3,4], Rémi Bardenet[5], Yi Cui[6], Jamie I. Vandenberg[3,4], David J. Gavaghan[1], Teun P. de Boer[7], Gary R. Mirams[1,8]

March 12, 2017

1. Computational Biology, Department of Computer Science, University of Oxford, OX1 3QD, UK.

2. Division of Applied Regulatory Science, Office of Clinical Pharmacology, Office of Translational Sciences, Center for Drug Evaluation and Research, Food and Drug Administration, Silver Spring, MD, USA.

3. Department of Molecular Cardiology and Biophysics, Victor Chang Cardiac Research Institute, Sydney, NSW 2010, Australia.

4. St Vincent's Clinical School, UNSW Sydney, Darlinghurst, NSW 2010, Australia.

5. CNRS & CRIStAL, Université de Lille, 59651 Villeneuve d'Ascq, France.

6. Safety Evaluation and Risk Management, Global Clinical Safety and Pharmacovigilance, GlaxoSmithKline, Uxbridge, UB11 1BS, UK.

7. Division of Heart & Lungs, Department of Medical Physiology, University Medical Center Utrecht, Utrecht, The Netherlands.

8. Centre for Mathematical Medicine & Biology, School of Mathematical Sciences, University of Nottingham, NG7 2RD, UK.

Abstract

Understanding the roles of ion currents is crucial to predict the action of pharmaceuticals and also to guide clinical interventions in the heart, brain and other electrophysiological systems. Our ability to predict how ion currents contribute to cellular electrophysiology is in turn critically dependent on the characterization of ion channel kinetics. We present a method for rapidly exploring and characterizing ion channel kinetics, using the hERG channel, responsible for cardiac I_{Kr} current, as an example. We fit a mathematical model to currents evoked by a novel 8 second sinusoidal voltage clamp. The model is then used to predict over 5 minutes of recordings in the same cell in response to further voltage clamp protocols, including a new collection of physiological action potentials. Our technique allows rapid collection of data from single cells, produces more predictive ion current models than traditional approaches, and will be widely applicable to many ion currents.

Keywords: hERG, I_{Kr}, mathematical model, cardiac, electrophysiology, parameter, inference, model validation, patch clamp, voltage-gated, ion channel, ion current, voltage protocol

1 Introduction

Mathematical models of ion channels are a quantitative expression of our understanding of the probability of the channel existing in different conformational states (typically, closed, open and inactivated) and the rates of transition between these states[1,2]. There have been some notable advances in deriving mathematical models for ion channel behavior[3–7], with some stressing the need for validation/testing of the model using data from the same cell[8]. In this paper we present a new approach, based on novel short protocols and parameter inference techniques, which we demonstrate by constructing an improved ion channel model.

The *KCNH2* gene (also known as *hERG*) has been shown to encode the primary subunit of the voltage-gated ion channel Kv11.1 that carries the rapid delayed rectifier potassium current (I_{Kr})[9,10]. In this article we focus on mathematical modeling of hERG channel kinetics, demonstrating our approach by constructing an improved model of this ion channel. hERG plays important roles in the brain[11]; gastrointestinal tract[12]; uterine contractions[13]; cell-proliferation and apoptosis[14] and cancer progression[15], but I_{Kr} is best known as a repolarizing cardiac ion current. The channel is susceptible to binding and blockade by pharmaceutical compounds, which is strongly linked to many cases of drug-induced pro-arrhythmic risk[16,17]. Mathematical modeling of cardiac electrophysiology, including I_{Kr}, forms a core part of a new proposal for routine *in vitro* and *in silico* safety assessment to replace a human clinical drug safety study[18,19]. A wide range of different mathematical models have been proposed to describe I_{Kr} (details of literature models are given in Supplementary Material B, Table B1). We note that these models were developed to describe different species, cell types, temperatures and isoforms, so variation is to be expected. Figure 1 shows predicted current under three different voltage clamps for 29 literature models. Unfortunately, even models for the same conditions do not provide consistent predictions.

The first models of ion channel kinetics were proposed by Hodgkin & Huxley[20], and relatively little has changed in the methods used for construction of mathematical models of ion channel gating since the original seminal work in 1952. The traditional approach is to fit peak currents and time constants of current activation/decay after clamping to fixed voltages; to assemble current/voltage (I–V) and time-constant/voltage (τ–V) curves; and to describe these curves with interpolating functions. Condensed voltage-step protocols have been suggested as the basis of optimized experiments that provide information about ion channel kinetics faster than experiments to construct I–V curves[21,22]; and optimized current and voltage step clamps have been used to optimize the fitting of maximal conductances in action potential models[23]. Single sinusoid voltage clamps have been previously been explored for choosing between possible Shaker channel models that were parameterized using traditional voltage step clamps[24].

In this study, we extend these ideas and propose an 8second sinusoid-based voltage protocol, designed to explore the kinetics of the hERG channel, and use this protocol to record hERG currents from CHO-cells that are over-expressing hERG1a. These recordings are then used to parameterize a mathematical model of the ion current. We then validate the model by predicting the response to both standard voltage-step protocols and physiologically-relevant action potential clamps: an unprecedentedly thorough independent validation for a model of ion channel kinetics. Our approach uses a substantially shorter experimental recording to construct the ion channel model than the usual approach based on time constants and peak currents from a series of voltage-step protocols. As a consequence of the high information content of the short protocol, we are able to generate cell-specific models that advance our understanding of variability of ion currents between cells. Our methodology will be applicable to many ion channels, both in the heart and other electrophysiological systems.

A

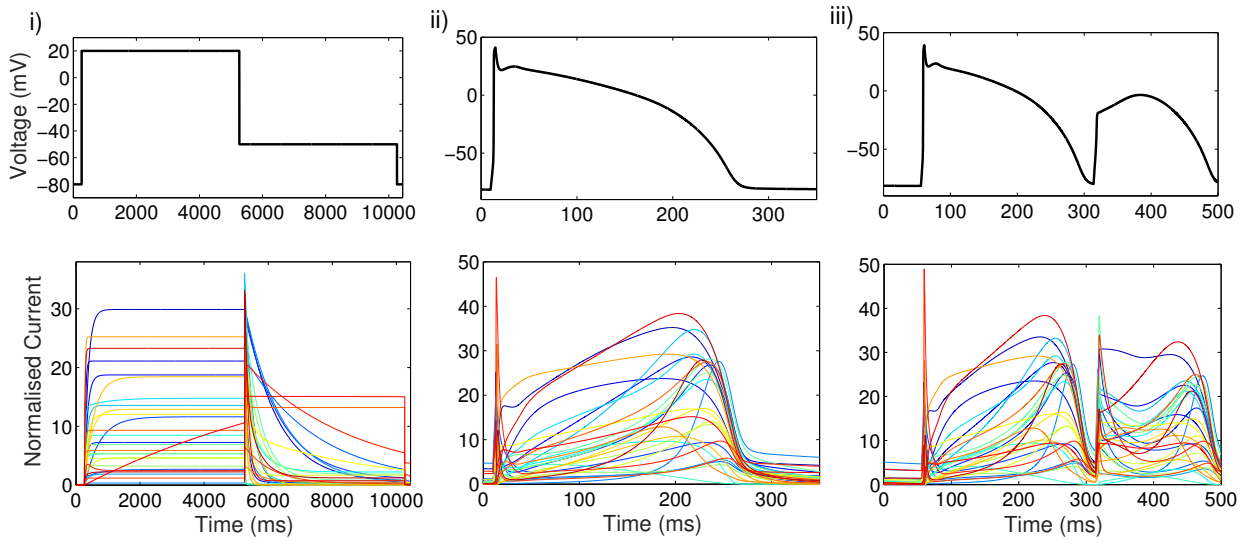

B

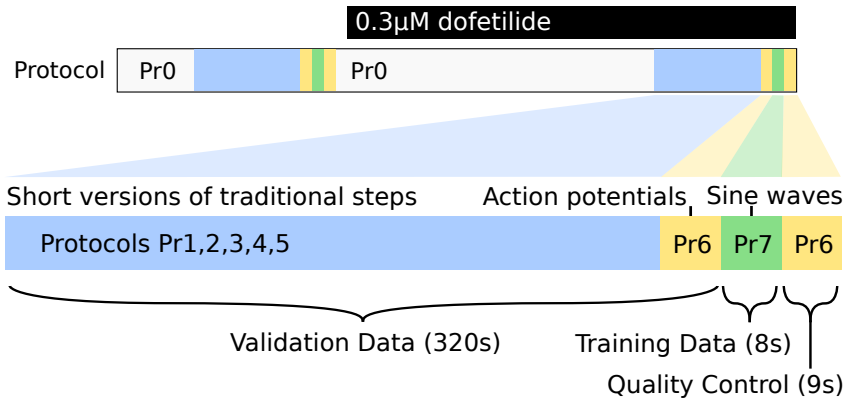

Figure 1: **Current predictions from literature models of I_{Kr}, and diagram of the experimental procedure used in this study**. **A:** predictions from 29 literature models of I_{Kr} in response to different voltage-clamp protocols: (i) a voltage-step; (ii) an action potential; and (iii) an action potential displaying pathological properties. Currents are normalized such that the maximal conductance is equal to one; i.e. we plot the open probability multiplied by the driving voltage (model references are listed in Table B1 in Supplementary Material B). **B:** top — a schematic representation of the experimental procedure used for this study over time (not to scale). A simple activation step protocol is repeated in the sections marked 'Pr0', before moving on to the highlighted section (enlarged below) where data used in the study were recorded. The recording protocols 'Pr1–7' are performed twice, once before dofetilide addition, and once after, with the hERG current isolated by subtraction. For full details of the protocols please refer to the Online Methods 4.2.

2 Results

2.1 Experimental Protocol

In Figure 1B we provide an overview of the experimental approach, denoting the sequence of voltage clamp protocols we performed as Pr0–Pr7. In each cell we recorded: a series of more conventional voltage-step protocols designed to explore activation (Pr1–3), inactivation (Pr4) and deactivation (Pr5); a new protocol composed of a series of action potential clamps (Pr6 — composed from simulated action potentials from models representing diverse species, pacing frequencies, and in both healthy and repolarization-failure conditions); and our new 8 s sinusoidal voltage protocol (Pr7, shown in Figure 2, full details of all protocols are given in the Online Methods 4.2).

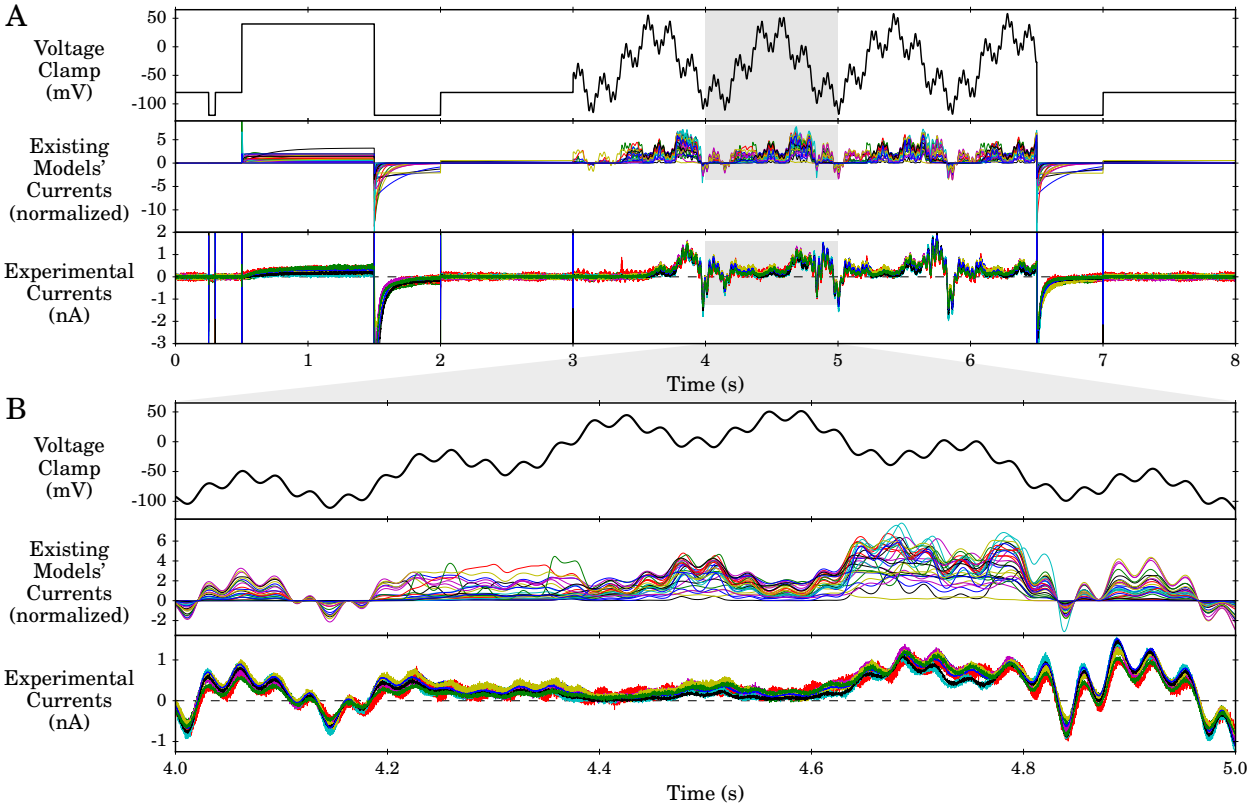

Figure 2: **The sine wave protocol and example recordings. A: Top row**: The full sinusoidal voltage protocol (Pr7). **Middle row**: Simulations of expected behavior in response to this protocol from existing I_{Kr} and hERG models, normalized by scaling the conductance value for each model to minimize the absolute difference between each trace and a reference trace. For calculation of the reversal potential, a temperature of 21.5 °C was used to match the mean experimental conditions. **Bottom row**: Raw data (following leak and dofetilide subtraction) from experimental repeats at room temperature from 9 cells. Experimental traces have been scaled, to remove the effect of different maximal conductances, by a factor chosen to minimize the absolute differences between each trace and a reference experimental trace (that with the peak current during the sine wave portion of the sine wave protocol). **B:** an enlargement of the highlighted sections of panel A. Whilst there is some variation between cells in the experimental results, they are much more consistent than the predictions from the different models.

In Figure 2 we present the novel sinusoidal protocol Pr7, the simulated predicted currents

from existing models, and the responses we recorded using the whole-cell patch clamp technique with hERG 1a-transfected CHO cells (details of the experimental methodology can be found in the Online Methods 4.1.1–4.1.3). The protocol is comprised of simple voltage steps and a main sinusoidal section that is in the form of a sum of three sine waves of different amplitudes and frequencies, here optimized to rapidly explore hERG channel kinetics. The steps are included to measure leak current and to provoke a large current to help identify maximal conductance (found to be helpful in preliminary work, see Supplementary Material A2.1). The frequencies of the sine waves are selected to cover the range of characteristic time constants known to occur in hERG channel gating (from millisecond to second timescales)[25,26], whilst avoiding harmonics that would lead to repetitive in-phase signals. The amplitudes of the sine waves are selected to sweep over physiological voltage ranges. Details of the protocol parameters and an equation for the protocol are given in Online Methods 4.2.

The sine wave protocol is of only eight seconds duration, which enables: efficient data collection, with training and validation data collected from the same cell; and the chance to make multiple interventions (such as the addition of drug compounds) since we can re-measure the full set of ion channel kinetics multiple times. The new protocol provokes from the existing literature I_{Kr} models an even wider array of different behaviors (middle panels in Figure 2A & B) than the existing voltage step or action potential clamps (Figure 1A); even among models constructed in/for similar conditions/species.

We recorded the full set of voltage protocols (Pr1–7) twice. After the first set of recordings, in vehicle conditions, we add a moderate dose of dofetilide (0.3 μM), allow the dofetilide-induced current block to reach equilibrium, and then repeat the full set of recordings. We leak-subtract each set of Pr1–7 recordings using the leak step at the beginning of Pr7 to estimate leak current resistance. Finally we subtract (the already leak-subtracted) second set of recordings from the first set, to obtain 'dofetilide subtracted' current traces, predominantly composed of dofetilide-sensitive hERG current. This procedure minimizes contributions from any endogenous currents (see Online Methods 4.4).

2.2 Model Calibration

We calibrate a mathematical model using only the sine wave protocol Pr7. The Hodgkin-Huxley[20] structure of the model we use, and its corresponding model parameters, can be seen in Figure 3B. We independently fitted this model to each of the experimental current traces shown in Figure 2. For each cell, we obtain a probability distribution of estimates for each parameter that captures any observational uncertainty in the parameter values[27,28]. We used a global minimization algorithm[29] followed by a custom-written Monte Carlo based Bayesian inference method (assuming uniform prior distributions, see Online Methods 4.7).

The result of the fitting procedure for one cell is shown in Figure 3. The parameter set with maximum posterior density is shown in Figure 3A, demonstrating an excellent fit between experimental and simulated data. The resulting posterior probability density for the parameters obtained from this Bayesian inference approach is projected across each parameter in Figure 3C. We also tested that our approach is theoretically appropriate for inferring all parameters by using synthetic data studies, as described in Supplementary Material C. The plausible parameter space is very narrow: if multiple parameter set samples are taken from the distribution shown in Figure 3C, the resulting simulated current traces are indistinguishable to the eye. To quantify this, taking 1000 samples we find that the 95% credible intervals for the simulated currents were always within at most either 3.45% or, in absolute terms, 0.0044 nA of the simulated current given by the maximum posterior density parameter set.

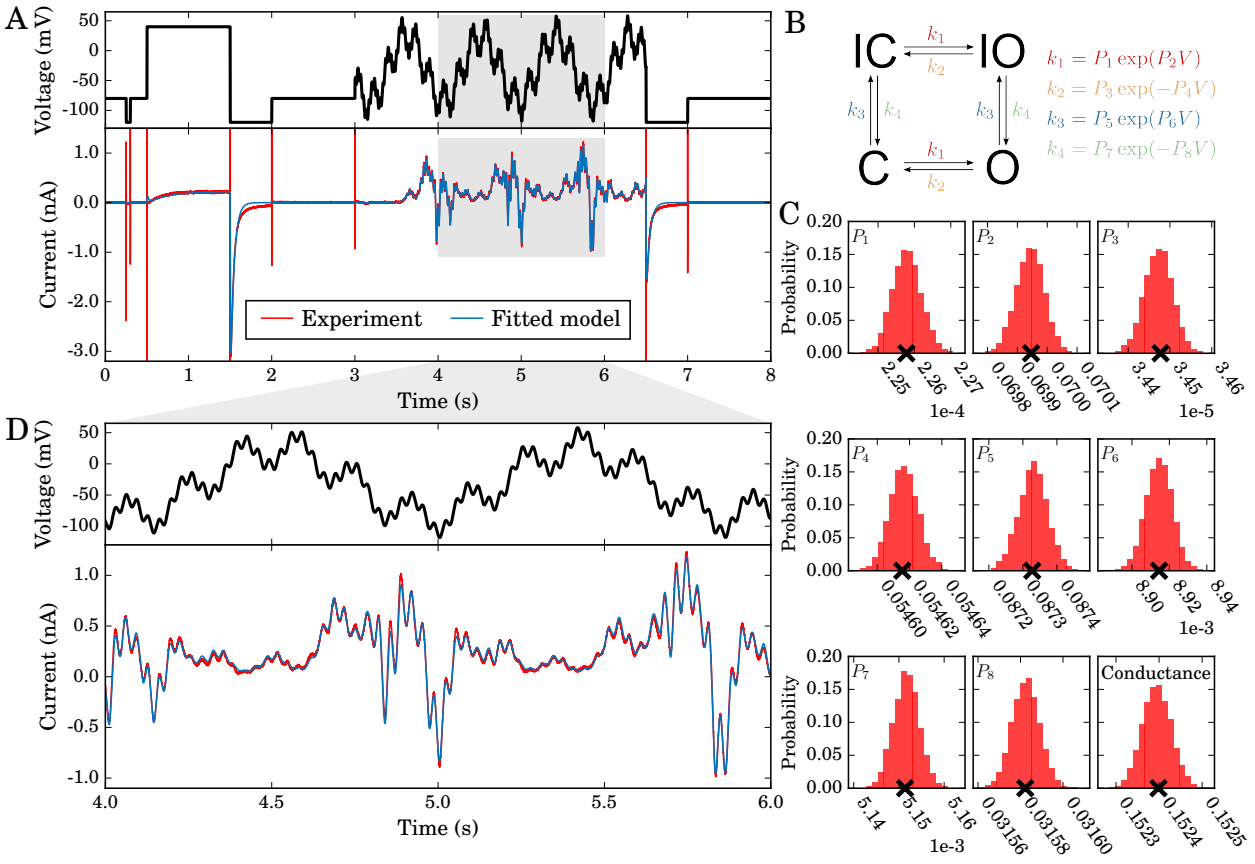

Figure 3: **Model calibration**. **A:** Top: the entire 8 second training protocol, bottom: an experimental recording with the fitted model simulation overlaid (portion of the sine wave enlarged in panel D). This simulation uses the maximum posterior density parameter set, denoted with crosses in panel C. **B:** The model structure in Markov state diagram format, note that the symmetric transition rates mean this is equivalent to a Hodgkin & Huxley[20]-style model with two independent gates. Parameter values P_1 to P_8 define voltage (V)-dependent transitions (k) between conformational states. **C:** posterior distribution of single-cell derived model parameters. Probability density distributions are shown for each parameter after fitting to the experimental data shown in panel A. The parameter numbering corresponds to that shown in panel B. Crosses indicate the parameter set with the maximum posterior density. The standard deviation of each of these distributions is less than 0.5% of the maximum posterior density value. **D:** an enlargement of the highlighted region of panel A.

The results we present in Figure 3 are from a single cell with a good quality recording and a high signal:noise ratio (this choice of cell, and other cells' predictions, are discussed later). We fit models on a cell-specific basis, and then also use averaged experimental data to create a single 'averaged' model as described in Supplementary Material F. We will compare these approaches below. We provide all parameter values with the maximum posterior density for all models in Supplementary Table F11.

2.3 Validation predictions

Having trained our model to eight seconds of experimental data from the sine wave protocol Pr7, we now test its ability to predict more than 5 minutes of independent experimental behavior. We predict the current in response to traditional voltage-step protocols Pr1–5 (adapted from those previously used in the literature[1]), and also to a novel physiologically-inspired voltage clamp protocol comprised of multiple action potentials (Pr6). All recordings shown in Figures 3–5 are from the same cell, using the experimental procedure shown in Figure 1B.

To make the predictions for Protocols Pr1–6 we performed simulations using the parameter set with the maximum posterior density in the fit to the sine wave (Pr7). As with the calibration protocol, all the predictions we will discuss below are indistinguishable by eye from the result of taking multiple samples from the distributions in Figure 3C and plotting a prediction for each of these parameter sets. We also compare the predictions from our new model with those from a sample of widely-used literature models[25,30–33].

In Figure 4, we show traditional voltage step protocols, experimental recordings and the simulated predictions from the model. We also show some of the usual summary curves of the data, together with predicted summary curves from our model and a range of existing literature models (methods used to derive summary plots are given in the Online Methods 4.5, results for Pr1&2 in Supplementary Material E). We can predict a wide range of current behavior in response to the standard voltage-step protocols, without having used any of this information to fit the model. Many of the current-voltage relationships and time constant-voltage relationships we predict in response to the traditional voltage-step protocols are closer to the experimental data than similar model-experiment comparisons in the literature (even when existing literature models, with more parameters, were fitted to similar data).

Figure 5 shows the model prediction of the currents invoked in response to the physiologically-inspired action potential protocol Pr6, compared with the experimental recording (as shown in Figure 1B we used the first repeat of Pr6 for validation purposes, and the second as a quality control measure). Replicating behavior under action potentials is perhaps the most important requirement for a hERG channel model for use in physiological or pharmacological studies. The model is able to predict the response to all of the complex action potential protocol extremely well, and much better than existing models (even though we have scaled literature models' maximal conductances (G_{Kr}) to fit this trace as well as possible in Figure 5).

We provide a quantitative comparison of predicted current traces for our model and each of the literature models for Pr3–7 in Supplementary Table D6. In each case, the worst-performing literature model is a Hodgkin-Huxley style model. Yet our simple model, with the same structure, is able to provide significantly better predictions than even the Markov-type models, which are usually considered to be better representations of hERG kinetics[1]. Our methodology has resulted in a simple and highly predictive mathematical model, able to describe a wide range of physiologically-relevant behavior.

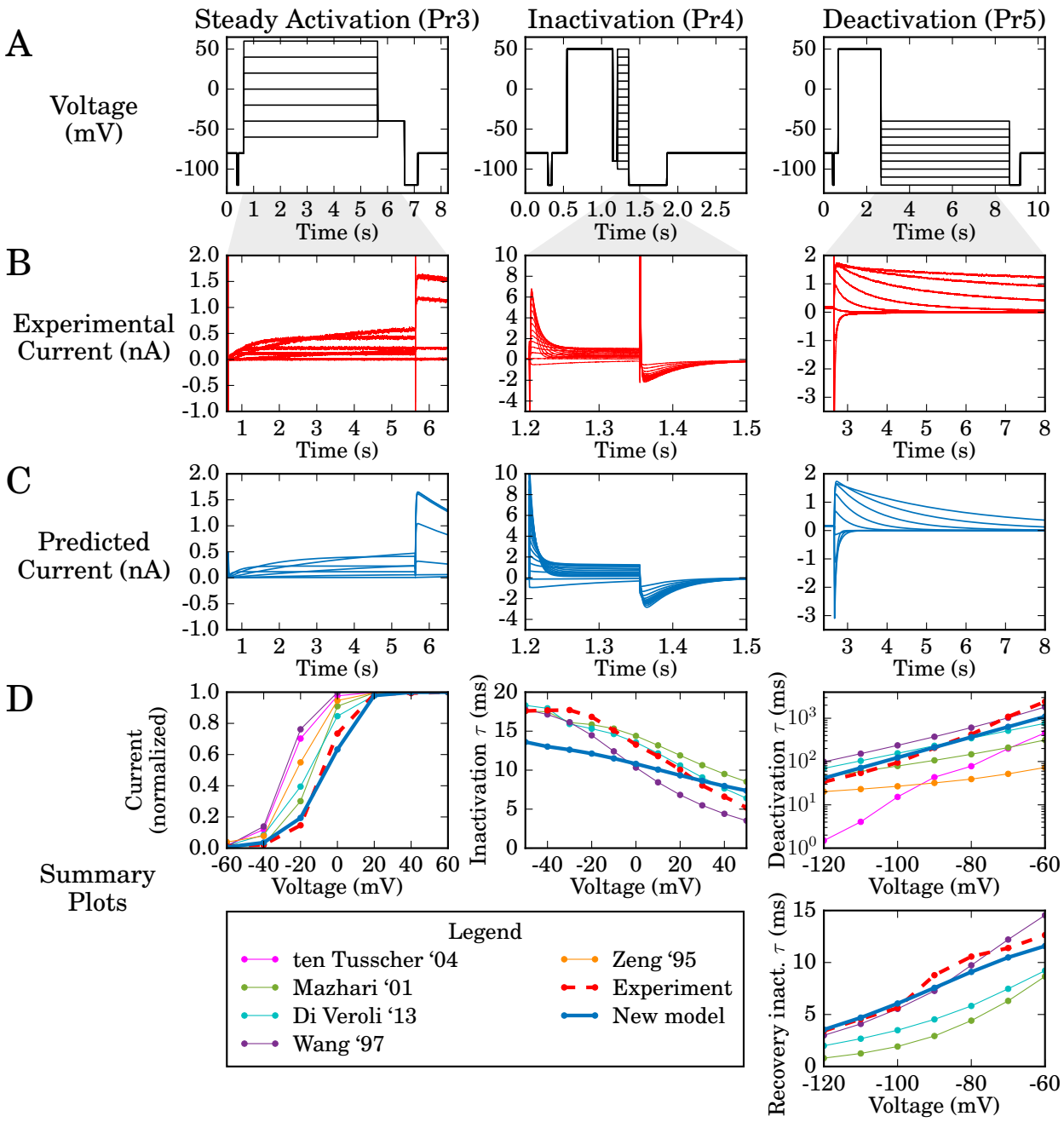

Figure 4: **Validation predictions — currents in response to traditional voltage step protocols**. Each column of graphs corresponds to a validation step protocol: those commonly used to study steady state activation, inactivation and deactivation (Pr3, Pr4, Pr5 in Figure 2) respectively. **A:** the voltage protocols. **B:** experimental current traces. **C:** model response — all are predictions using the maximum posterior density parameter set indicated in Figure 3C calibrated to just the sine wave protocol. **D:** summary curves, either current–voltage (I–V) or time constant–voltage (τ-V) relationships. These plots summarize the results in the relevant column. The model prediction is shown in blue bold throughout, and the experimental recording with a dashed red line. Note that the deactivation time constant we plot here is a weighted tau, described in Online Methods 4.5. Note that some literature model predictions are missing from the summary plots as we were either unable to fit exponential curves to 'flat' simulation output reliably; or the exponential decay occurred in the opposite direction to experimental traces, and we considered the comparison unwarranted.

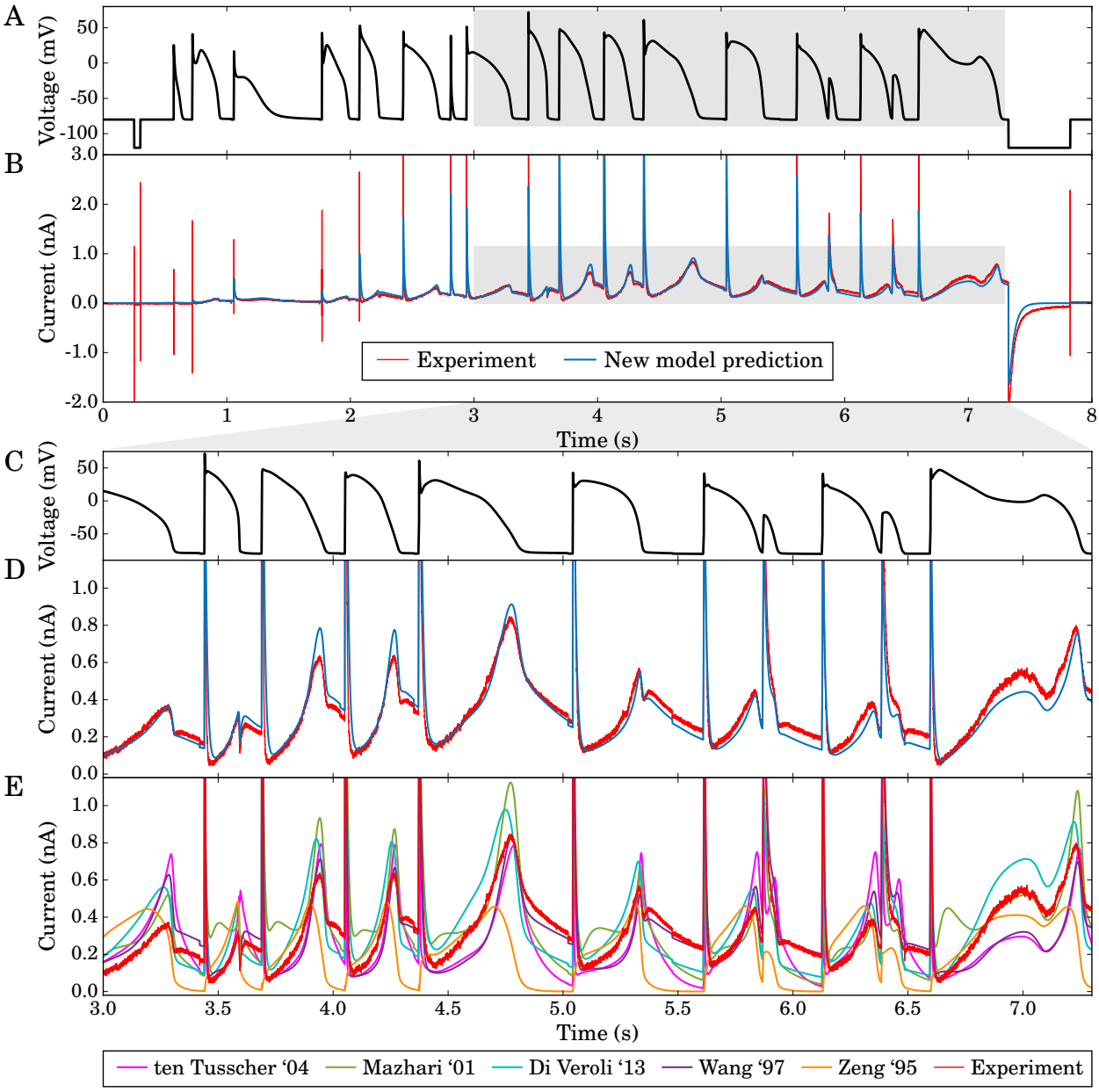

Figure 5: **Validation prediction — the current in response to the action potential protocol**. **A:** the voltage clamp protocol. **B:** a comparison of the experimental recording (red) and new model prediction (blue). **C & D:** enlargements of the highlighted regions of panels A & B. **E:** the same view of the experimental data in panel D, but here compared with predictions from literature I_{Kr} models. Conductance, G_{Kr}, is scaled for each of the literature models to give the least square difference between their prediction and these experimental data, i.e. we display a best-case scaling for each of these models. A quantification of the error in our model prediction versus these literature models is given in Supplementary Table D6: the performance shown in panels D and E holds for the whole trace, so the mean error in predicted current across the whole protocol is between 18% and 211% larger for the literature models' predictions than for our sine-wave fitted model.

2.3.1 Cell-specific validation

In Figure 6A we present the maximum posterior density parameter values when repeating the above approach using data from nine different cells. The clustered parameter values demonstrate that parameters derived from different cells take similar values, giving us confidence that the procedure is reproducible and biophysically meaningful. There is more cell-to-cell variability in some parameters than others, which may be related to variability in the underlying physiological processes that they represent; supporting the value, and perhaps necessity, of a cell-specific approach. We also acknowledge that some parameters may be more or less sensitive to variability in experimental conditions such as temperature, residual background/endogenous currents, and imperfect dofetilide and/or leak subtraction.

We order the cells in Figure 6 based on the lowest difference in leak resistance between the vehicle and dofetilide recordings of Pr7. This ordering gives a measure of recording stability, and is intended to be a surrogate for data quality. The cell presented above, in Figures 3–5, corresponds to Cell #5 of 9 under this ranking, so we obtain very good predictions even with our 'median' quality data. We show cell-specific predictions of the current-voltage relationship for the peak steady-state activation current for each cell-specific model in Figure 6B. While we focus on Cell #5 in the main text, Cells #1–4 also produce excellent cell-specific predictions (similar comparisons for other summary plots are in Supplementary Figures F8–F10).

We also investigated the benefit in a cell-specific approach by building a model using averaged experimental data from all nine cells. We describe this approach in Supplementary Material F, and summarize the results in Supplementary Table F12. Generally, for the cells with the highest data quality (Cells #1–5) the cell-specific models provide better predictions than the average model, as we see for Pr4 when comparing colored cell-specific predictions and experiment with the black line for the average model in Figure 6B. The same trend holds for the action potential protocol Pr6, in 6/9 cells the cell-specific model provides less error than the average cell model — the largest improvement was 37% less error; for the remaining 3/9 cells where the average cell model provided better predictions, this was by at most 6%.

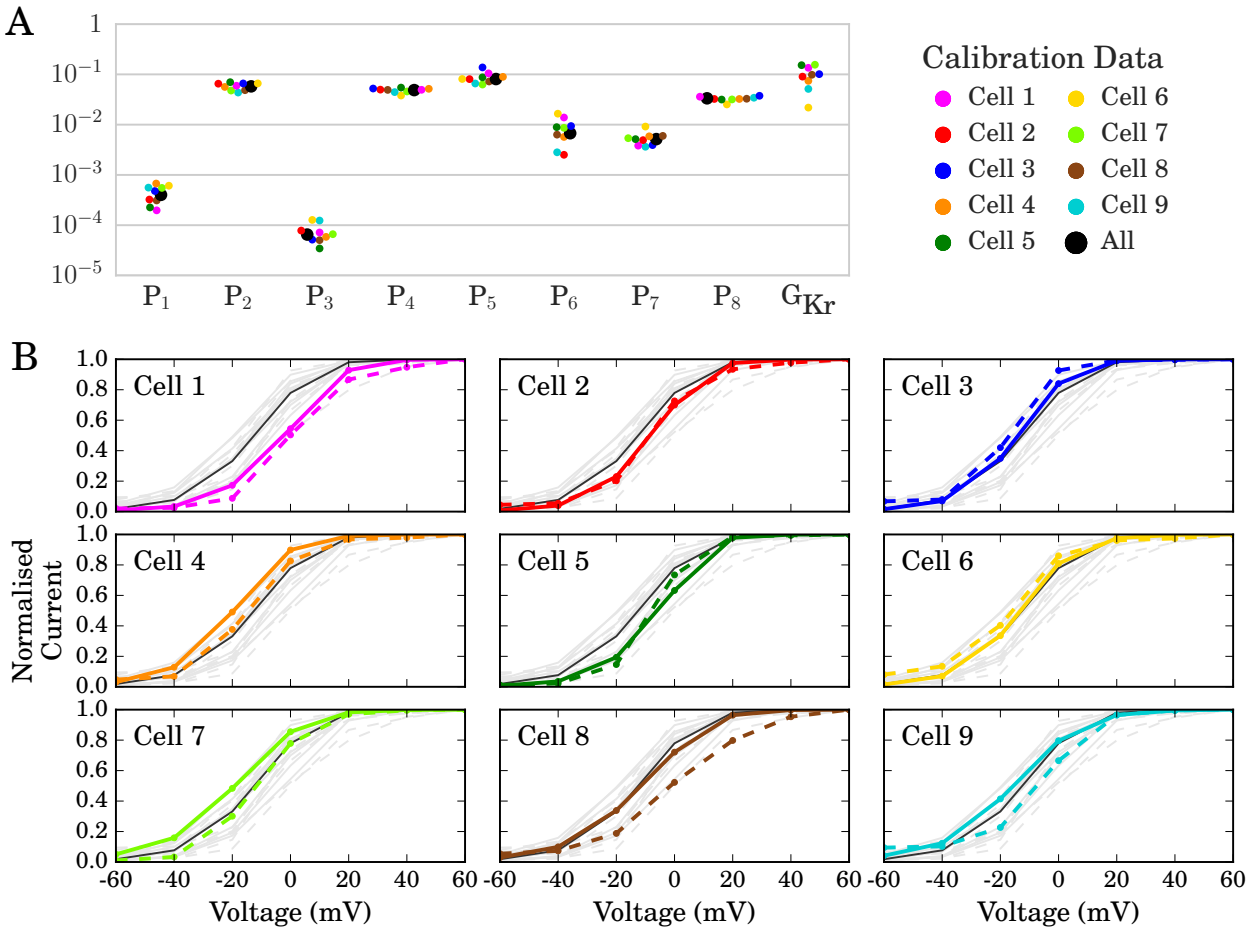

Figure 6: **Cell-specific model parameters, and comparison of their predictions with cell-specific experimental results**. (**A:**) Plot of parameters (maximum posterior density values) for nine cells obtained from training the model to the sinusoidal voltage protocol recorded on nine different cells, together with parameters calibrated to average data (N.B. not the average of the cell-specific parameters). The full set of parameter values are shown in Supplementary Material Table F11 and the distributions for each parameter shown in Figure F7. (**B:**) Comparison of cell-specific model predictions to cell-specific experimental recordings for the steady-state peak current I–V curves. Each plot represents a different cell, model predictions are depicted by a bold colored line, and dashed lines show values derived from the experimental data. The black lines (same on each plot) represent the prediction from the model calibrated to averaged data (all of the cells' data). Each subplot contains all of the other cells' recordings and predictions in light grey in the background to aid comparison and show the spread that we observed.

3 Discussion

In this paper we have presented a novel method for constructing mathematical models of ion channel kinetics. We used a sinusoidal voltage protocol to construct a simple model of hERG channel kinetics using just 8 seconds of recording, as opposed to a traditional approach that requires several minutes of voltage-step data. All of our experimental data can be collected from a single cell, whereas a typical approach necessitates the collection of data from a number of different cells.

The conceptual shift is that channel kinetics should be summarized by mathematical model parameters, not a series of current-voltage (I–V) and time constant-voltage curves. In essence, the model *is* the current characterization, rather than something designed to fit I–V and time constant curves, which only represent a certain subset of possible behaviors of the current. By fitting directly to the experimental current traces, instead of using summary curves, we can also reduce the possible influence of subjective choices during the time-constant fitting process.

We saw that our model is able to replicate the experimental training data very well (Figure 3). This is often the point at which literature approaches stop and conclude that a mathematical model is a good representation of ion channel kinetics (something that is also true more generally for mathematical models of biological processes). Instead, we performed an unprecedentedly thorough evaluation of the model by testing its ability to predict the behavior in response to a series of voltage clamp protocols it has not 'seen before' (both those traditionally used to characterize hERG channel kinetics, and also a new complicated series of action potential waveforms), all recorded from the same cell as the training data. The extremely good prediction from all our cell-specific models of the response to the complex action potential protocol is particularly remarkable (Figure 5). We are not aware of such a thorough, physiologically-relevant validation of an ion channel model having been performed before. Testing that we are able to predict the current response to a voltage pattern which may be observed in physiological or patho-physiological conditions is a particularly robust and useful way to validate a model, and critical if the I_{Kr} model is to be used to accurately predict cardiac electrical activity in healthy and potentially arrhythmic situations.

There are still some aspects of the experimental behavior that are not replicated by our model. In particular, there is only one time constant of deactivation, and low voltage-dependence in the inactivation time constant (Figure 4). But then neither is the full range of behavior captured by any of the existing, more complex, models available in the literature; and we have shown that our model can provide better predictions of all the raw currents than the literature models in the majority of cases, even where summary curves are not predicted as accurately. The inability of our model to replicate all of the experimental data may be a consequence of using a simple Hodgkin-Huxley model formulation, although it is a commonly used structure for currents within action potential models.

However, the simplicity of our model may also be the key to its success — with only eight kinetic parameters we have confidence that they are all being fitted well, and we have shown that there is low uncertainty in their values. As Pathmanathan & Gray[27] and Mirams *et al.*[28] have recently discussed, considering probabilistic uncertainty in our model parameters and predictions is evermore important as models begin to be used for safety-critical predictions such as the CiPA initiative[18,19] and clinical applications[34].

A key limitation of our approach is that experiments have been performed in expression line cells, creating a hERG1a model; compared to native I_{Kr} current in cardiac cells which will have additional isoforms, subunits and regulation. To characterize I_{Kr} kinetics we plan to apply the methodology presented here in native myocytes, to make a model that is more applicable for use in cardiac safety testing and whole-organ simulations.

The success of our approach in different ion channels will be heavily dependent on the precise

form of the sinusoidal protocol that is used, and in parallel work we are developing different strategies for optimizing the voltage protocol design for given currents. Previously, Bett *et al.*[1] explored the behaviors of a subset of existing hERG channel models and concluded that the model proposed by Wang *et al.*[25] was best able to replicate the activation kinetics of the hERG channel. In parallel work, we are extending the approach presented here for selecting and calibrating the most appropriate model structure for hERG channel kinetics (see Supplementary Material Figure B4 for the range of possibilities).

We have demonstrated the advantages of a cell-specific mathematical modeling approach, observing an overall improvement in model predictions using cell-specific models relative to a model made using averaged data. The approach therefore allows, for perhaps the first time, an exploration of both within-cell and between-cell variability in ion channel kinetics. The cell-specific predictions are particularly strong when using the highest quality data, highlighting the necessity of maintaining very high data quality for constructing accurate and robust mathematical models of ion channel kinetics.

The significant time saving of our short protocol opens up the possibility of taking more recordings in different experimental conditions within a single cell (e.g. drug concentrations[35,36] or temperatures[37]), leading to datasets that are more consistent, and therefore of higher quality. These datasets will result in more accurate mathematical descriptions of ionic currents in these different conditions. The approach we have presented allows more predictive mathematical models of ion channel kinetics to be formulated, which will lead to more accurate predictions of ion currents in different organ systems.

Acknowledgments

Our thanks to Prof. Gail Robertson of University of Wisconsin–Madison for assistance in acquiring the cell line used in pilot stages of this study. We would also like to thank the following people for technical assistance, access to facilities, support and encouragement: Jim Louttit, Nick McMahon, Carol Wilson, Sam Turner, Kate Harris and Sara Graham of GSK Safety Assessment; Jules Hancox of University of Bristol; Monique Windley and Mark Hunter of Victor Chang Cardiac Research Institute; Rianne Rijken and Birgit Goversen of UMC Utrecht. Thanks to Ross Johnstone (University of Oxford) for removing singularities from the Zeng model, and to Frank Ball (University of Nottingham) for comments on a paper draft.

KAB was supported by the EPSRC and GlaxoSmithKline Plc (grant numbers EP/G037280/1, EP/I017909/1 and EP/K503769/1). JIV and APH acknowledge funding from the NHMRC. RB acknowledges support from ANR grant BoB ANR-16-CE23-0003. GRM gratefully acknowledges support from a Sir Henry Dale Fellowship jointly funded by the Wellcome Trust and the Royal Society (grant number 101222/Z/13/Z).

Author Contributions

KAB, RB, YC, DJG, TdeB, GRM designed the study and modeling approach; KAB, RB & GRM designed and implemented the statistical methods; KAB, GRM, JIV, APH and TdeB designed and refined the experimental methods; KAB performed all the experiments, simulations and statistical analysis; KAB, TdeB, GRM wrote the manuscript; all authors approved the final version of the manuscript.

Competing Financial Interests

The authors declare that the research was conducted in the absence of any commercial or financial relationships that could be construed as a potential conflict of interest.

Disclaimer

The opinions presented here are those of the authors. No official support or endorsement by the Food & Drug Administration is intended nor should be inferred.

Materials & Correspondence

All computational codes, and the experimental current recordings that were used for calibration and validation (leak and dofetilide subtracted), are openly available in a Supplementary Data repository at `https://github.com/mirams/sine-wave`. A permanently archived version is available on Figshare at `https://doi.org/10.6084/m9.figshare.4704550.v2` alongside the full raw data (in both plain text and PClamp formats) at `https://doi.org/10.6084/m9.figshare.4702546.v1`.

K.A.B. is the corresponding author.

References

1. Bett, G. C., Zhou, Q. & Rasmusson, R. L. Models of HERG Gating. *Biophysical Journal* **101,** 631–642 (2011).
2. Vandenberg, J. *et al.* hERG K+ channels: Structure, function, and clinical significance. *Physiological Reviews* **92,** 1393–1478 (2012).
3. Balser, J. R., Roden, D. M. & Bennett, P. B. Global parameter optimization for cardiac potassium channel gating models. *Biophysical journal* **57,** 433–44 (Mar. 1990).
4. Cannon, R. C. & D'Alessandro, G. The ion channel inverse problem: neuroinformatics meets biophysics. *PLoS Comput Biol* **2,** e91 (2006).
5. Siekmann, I. *et al.* MCMC estimation of Markov models for ion channels. *Biophysical journal* **100,** 1919–29 (Apr. 2011).
6. Siekmann, I., Sneyd, J. & Crampin, E. J. MCMC can detect nonidentifiable models. *Biophysical journal* **103,** 2275–86 (Dec. 2012).
7. Loewe, A. *et al.* Parameter Estimation of Ion Current Formulations Requires Hybrid Optimization Approach to Be Both Accurate and Reliable. *Frontiers in bioengineering and biotechnology* **3,** 209 (Jan. 2015).
8. Tomaiuolo, M., Bertram, R., Leng, G. & Tabak, J. Models of Electrical Activity: Calibration and Prediction Testing on the Same Cell. *Biophysical Journal* **103,** 2021–2032 (2012).
9. Trudeau, M. C., Warmke, J. W., Ganetzky, B. & Robertson, G. A. HERG, a human inward rectifier in the voltage-gated potassium channel family. *Science* **269,** 92 (1995).
10. Sanguinetti, M., Jiang, C., Curran, M. & Keating, M. A mechanistic link between an inherited and an acquired cardiac arrthytmia: HERG encodes the IKr potassium channel. *Cell* **81,** 299–307 (1995).
11. Babcock, J. J. & Li, M. hERG channel function: beyond long QT. *Acta Pharmacologica Sinica* **34,** 329–35 (2013).

12. Farrelly, A. M. *et al.* Expression and function of KCNH2 (HERG) in the human jejunum. *American journal of physiology. Gastrointestinal and liver physiology* **284,** G883–95 (2003).

13. Parkington, H. C. *et al.* Diminished hERG K+ channel activity facilitates strong human labour contractions but is dysregulated in obese women. *Nature communications* **5,** 4108 (2014).

14. Jehle, J., Schweizer, P. A., Katus, H. A. & Thomas, D. Novel roles for hERG K(+) channels in cell proliferation and apoptosis. *Cell death & disease* **2,** e193 (2011).

15. Lastraioli, E. *et al.* hERG1 channels drive tumour malignancy and may serve as prognostic factor in pancreatic ductal adenocarcinoma. *British Journal of Cancer* **112,** 1076–87 (2015).

16. Redfern, W. *et al.* Relationships between preclinical cardiac electrophysiology, clinical QT interval prolongation and torsade de pointes for a broad range of drugs: Evidence for a provisional safety margin in drug development. *Cardiovascular Research* **58,** 32 (2003).

17. Pollard, C. E. *et al.* An introduction to QT interval prolongation and non-clinical approaches to assessing and reducing risk. *British Journal of Pharmacology* **159,** 12–21 (2010).

18. Sager, P., Gintant, G., Turner, J., Pettit, S. & Stockbridge, N. Rechanneling the cardiac proarrhythmia safety paradigm: a meeting report from the Cardiac Safety Research Consortium. *American Heart Journal* **167,** 292–300 (2014).

19. Fermini, B. *et al.* A New Perspective in the Field of Cardiac Safety Testing through the Comprehensive In Vitro Proarrhythmia Assay Paradigm. *Journal of Biomolecular Screening* **21,** 1–11 (2016).

20. Hodgkin, A. L. & Huxley, A. F. A quantitative description of membrane current and its application to conduction and excitation in nerve. *J. Physiol.* **117,** 500–544 (1952).

21. Hobbs, K. H. & Hooper, S. L. Using complicated, wide dynamic range driving to develop models of single neurons in single recording sessions. *Journal of Neurophysiology* **99,** 1871–1883 (2008).

22. Fink, M. & Noble, D. Markov models for ion channels: versatility versus identifiability and speed. *Philosophical Transactions of the Royal Society A* **367,** 2161–2179 (2009).

23. Groenendaal, W. *et al.* Cell-Specific Cardiac Electrophysiology Models. *PLoS Computational Biology* **11,** e1004242 (Apr. 2015).

24. Kargol, A., Hosein-Sooklal, A., Constantin, L. & Przestalski, M. Application of oscillating potentials to the Shaker potassium channel. *General Physiology and Biophysics* **23,** 53–76 (2004).

25. Wang, S., Liu, S., Morales, M., Strauss, H. & Rasmusson, R. A quantitative analysis of the activation and inactivation kinetics of HERG expressed in Xenopus oocytes. *The Journal of Physiology* **502,** 45–60 (1997).

26. Zhou, Z. *et al.* Properties of HERG channels stably expressed in HEK 293 cells studied at physiological temperature. *Biophysical Journal* **74,** 230–241 (1998).

27. Pathmanathan, P. & Gray, R. A. Ensuring reliability of safety-critical clinical applications of computational cardiac models. *Frontiers in Physiology* **4,** 1–9 (2013).

28. Mirams, G. R., Pathmanathan, P., Gray, R. A., Challenor, P. & Clayton, R. H. White paper: Uncertainty and variability in computational and mathematical models of cardiac physiology. *The Journal of Physiology* **594,** 6833–6847 (2016).

29. Hansen, N., Muller, S. & Koumoutsakos, P. Reducing the time complexity of the derandomized evolution strategy with covariance matrix adaptation (CMA-ES). *Evolutionary Computation* **11,** 1–18 (2003).

30. Zeng, J., Laurita, K. R., Rosenbaum, D. S. & Rudy, Y. Two components of the delayed rectifier K+ current in ventricular myocytes of the guinea pig type theoretical formulation and their role in repolarization. *Circulation Research* **77,** 140–152 (1995).

31. Mazhari, R., Greenstein, J., Winslow, R., Marbán, E. & Nuss, H. Molecular interactions between two Long-QT syndrome gene products, HERG and KCNE2, rationalized by in vitro and in silico analysis. *Circulation Research* **89,** 33–38 (2001).

32. Ten Tusscher, K., Noble, D., Noble, P. & Panfilov, A. A model for human ventricular tissue. *American Journal of Physiology-Heart and Circulatory Physiology* **286,** H1573–H1589 (2004).

33. Di Veroli, G., Davies, M., Zhang, H., Abi-Gerges, N. & Boyett, M. High-throughput screening of drug-binding dynamics to HERG improves early drug safety assessment. *American Journal of Physiology-Heart and Circulatory Physiology* **304,** H104–H117 (2013).

34. Arevalo, H. J. *et al.* Arrhythmia risk stratification of patients after myocardial infarction using personalized heart models. *Nature communications* **7** (2016).

35. Pearlstein, R. A. *et al.* Implications of Dynamic Occupancy, Binding Kinetics, and Channel Gating Kinetics for hERG Blocker Safety Assessment and Mitigation. *Current Topics in Medicinal Chemistry* **16,** 1792–818 (2016).

36. Lee, W. *et al.* In silico assessment of kinetics and state dependent binding properties of drugs causing acquired LQTS. *Progress in biophysics and molecular biology* **120,** 89–99 (2016).

37. Vandenberg, J. I. *et al.* Temperature dependence of human ether-a-go-go-related gene K+ currents. *American journal of physiology. Cell physiology* **291,** C165–75 (2006).

4 Online Methods

4.1 Experimental methods

4.1.1 Cell Culture

Chinese Hamster Ovary (CHO) cells stably expressing Kv11.1 were used in the patch clamp experiments performed in this study. Cells were cultured in Ham's F12 nutrient mix containing 5% fetal bovine serum and maintained at 37°C with 5% CO_2.

4.1.2 Electrophysiology Solutions

The bath solution was composed of: NaCl (137 mM), KCl (4 mM), $MgCl_2$ (1 mM), HEPES (10 mM), glucose (10 mM), and $CaCl_2$ (1.8 mM). The pH of the solution was adjusted to 7.4 with NaOH. Borosilicate glass micropipettes were pulled and fire polished to final tip resistances of approximately 2–5 MΩ when filled with pipette solution containing: KCl (130 mM), $MgCl_2$ (1 mM), HEPES (10 mM), EGTA (5 mM), and MgATP (5 mM). pH of the solution was adjusted to 7.2 with KOH. All experiments were performed at room temperature (21–22°C). Using this temperature and the composition of the bath and pipette solutions, a K^+ reversal potential of approximately -88.4 mV was calculated using the Nernst potential (equation (8)), the exact value depending on the particular temperature of each experimental recording.

4.1.3 Recording Techniques

Current recordings were made using an Axopatch 200B amplifier in whole-cell patch clamp mode. Data acquisition was performed using pClamp 10 software (Molecular Devices, Sunnyvale, USA). The protocols were first created as text files and then converted to `.abf` stimulus files to make corresponding `.pro` protocol files in the pClamp 10 software. A CV 203BU amplifier headstage and a Digidata 1440A were used. A Sutter MP225 micromanipulator was used for positioning of the microelectrode. The current signal was sampled at a rate of 10 kHz. 75–80% series resistance compensation was applied and data were 5 kHz low pass Bessel filtered by the hardware. No software filtering was applied. Whole-cell capacitance compensation was applied electronically. Leak subtraction was applied offline by using a 50 ms leak step to allow correction. To make a series of successive recordings using different protocols on the same cell, the pClamp "Sequencing Keys" tool was utilized, with a `.sks` file detailing the sequence the protocols should be performed in.

4.2 Experimental Protocols

For each cell we recorded a series of standard voltage-step protocols, a protocol comprised of a series of action potentials and the sine wave protocol, as shown schematically in Figure 1B. In all protocols the holding potential was initially held at −80 mV before applying a 50 ms leak step to −120 mV before returning back to −80 mV, with this step being used to estimate the leak current (as described in Section 4.3). Note that the 'standard' voltage-step protocols we have used to test our approach are shorter than some of those which have previously been used to calibrate mathematical models (with fewer test voltages/timings used) in order to perform them all in a single cell, with and without dofetilide subtraction, so a 'traditional approach' would take longer than the experiment performed here, perhaps requiring multiple cells. The voltage step to −120 mV at the end of all the protocols ensures that channels close quickly, reducing the time needed between protocols to regain a steady closed state.

Protocol 0 — Repeated activation step

Before the start of each set of recordings on each cell an activation step protocol with a start-to-start interval of 12 seconds was repeated several times until consistent currents were observed on each repeat. From an initial holding potential of −80 mV, this protocol comprised a 5 s step to 10 mV followed by a 5 s step to −50 mV before returning again to a holding potential of −80 mV. This protocol is depicted in Supplementary Figure A1. We repeated this protocol while dofetilide was added (see Figure 1B) and the current traces recorded from this protocol were used to assess when a steady level of dofetilide block had been reached.

Protocols 1,2 — Activation Kinetics

After the initial period at holding potential incorporating the −120 mV leak step, a step to V_{step_1} followed and was held at that voltage for T_{step} ms, before a step to −120 mV for 2.5 s, before returning to holding potential of −80 mV for 1 second. The protocol was repeated 6 times with a different T_{step} on each repeat. T_{step} took the values of 3, 10, 30, 100, 300 and 1000 ms.

- For Protocol 1, V_{step_1} is 0 mV. This protocol is depicted in Supplementary Figure A2.
- For Protocol 2, V_{step_1} is +40 mV. This protocol is depicted in Supplementary Figure A3.

Protocol 3 — Steady-State Activation

From the initial period at holding potential incorporating the −120 mV leak step, a step to V_{step} was applied for 5 seconds, followed by a 1 s step to −40 mV, before a 500 ms step to −120 mV, and then returning back to holding potential for one second. This process was repeated 7 times with a different V_{step} on each repeat. V_{step} ranged from −60 mV to +60 mV in 20 mV increments. This protocol is depicted in Figure 4A (left column).

Protocol 4 — Inactivation

From the initial period at holding potential incorporating the −120 mV leak step, a step to 50 mV for 600 ms, and a step to −90 mV for 60 ms, followed by a step to V_{step} for 150 ms, before a 500 ms step to −120 mV, and a 1 s step back to holding potential of −80 mV; This was repeated 16 times with a different V_{step} on each repeat. V_{step} ranged from −100 mV to 50 mV in 10 mV increments. This protocol is depicted in Figure 4A (middle column).

Protocol 5 — Deactivation

From the initial period at holding potential incorporating the −120 mV leak step, a step to 50 mV for 2 s was applied, followed by a step to V_{step} for 6 s, before a 500 ms step to −120 mV, and then returning back to holding potential for one second. This process was repeated 9 times with a different V_{step} on each repeat. V_{step} ranged from −120 mV to −40 mV in 10 mV increments. This protocol is depicted in Figure 4A (right column).

Protocol 6 — Action Potentials

This protocol was formed by combining a series of different simulated action potentials from the Cardiac Electrophysiology Web Lab[38] (and we added some simulated action potentials where early after depolarizations and delayed after depolarizations had been induced). The range of models we used for the simulations encompassed different cell types and species, the action potentials were

shifted slightly so that their resting potentials were exactly −80 mV (see the Supplementary Code for full details and code to reproduce this protocol).

Protocol 7 — Sine Wave Protocol

The training protocol took the form of 250 ms at holding potential of −80 mV, followed by a 50 ms leak step to −120 mV, and then 200 ms back at −80 mV. This was followed by a 1 s step to 40 mV, and a 500 ms step to −120 mV, before returning to −80 mV for 1 second. The 3.5 s sine wave portion of the protocol then followed (the form of which is described below), before a 500 ms step to −120 mV, and a return to −80 mV for 1 s.

The sine wave portion of the protocol takes the form of a sum of three sine waves as shown in Equation 1.

$$V(t) = -30 + A_1 \sin(2\pi\omega_1(t - 2500)) + A_2 \sin(2\pi\omega_2(t - 2500)) + A_3 \sin(2\pi\omega_3(t - 2500)), \quad (1)$$

where $A_1 = 54\,\text{mV}$, $A_2 = 26\,\text{mV}$, $A_3 = 10\,\text{mV}$, $\omega_1 = 0.007/(2\pi)$, $\omega_2 = 0.037/(2\pi)$ and $\omega_3 = 0.19/(2\pi)$, and t is time measured in milliseconds.

The protocol was initially designed with just the −120 mV leak step and not the additional steps to 40 mV and −120 mV (which were included after preliminary experiments as described in Supplementary Material A2.1) and so the sine wave was shifted by −2500 ms (as shown in equation (1)) to begin at the same phase after we incorporated the additional steps.

All of the protocols described in this section were adjusted on the amplifier to account for the liquid junction potential which was calculated to be 4.1 mV from the ionic composition of our physiological solutions which are described in Section 4.1.2. The liquid junction potential was calculated using the junction potential calculator in the pClamp software.

4.3 Leak Correction

We used the leak-step from −80 mV to −120 mV in order to leak-correct the experimental data, according to:

$$I_{\text{corrected}} = I_{\text{raw}} - V/R_{\text{leak}}. \quad (2)$$

Leak subtraction was performed using a MatLab script written for this purpose. We identified the most appropriate R_{leak} value to minimize the difference between the mean current value during the leak step (to −120 mV) compared to the mean value at a holding potential of −80 mV, whilst ensuring that the trace was not over-corrected (which would result in negative currents during the initial stages of activation). We manually selected leak resistances to correct the current evoked by the sine wave protocol in both vehicle and dofetilide conditions. We then applied this leak resistance to the remaining protocols performed in the same condition on each cell. The mean current during the −80 mV step was calculated from 200 ms of the −80 mV holding period before the −120 mV leak step (not including the capacitive spike at the point at which the step occurs). The baseline current at a holding potential of −80 mV was then adjusted back to 0 nA with a constant additive current if required.

4.4 Dofetilide Subtraction

In preliminary work in HEK cells we observed that our sine wave protocols could elicit endogenous currents, potentially interfering with the predictive ability of the resulting mathematical models. To overcome this technical issue we first constrained the design of the sine wave protocol so that only voltages within a physiological range of −120 mV to +60 mV were explored. In addition, we

repeated all the voltage protocols described above both in vehicle conditions and in the presence of 0.3 μM dofetilide. We then subtracted the currents remaining in the presence of the moderate dose of dofetilide from those recorded in the vehicle to remove any contribution of endogenous currents (and to produce what we refer to as 'dofetilide subtracted' data). Prior to performing this subtraction, we first leak subtracted both the vehicle and dofetilide recordings individually, as described above.

The required dose of dofetilide was obtained by serial dilution. Dofetilide was first dissolved in Dimethyl sulfoxide (DMSO) before being added to the bath solution to produce the required concentrations.

We observed that the levels of endogenous currents the protocols elicited varied from cell to cell (and were generally much lower in the CHO cells used in this study than in the HEK cells used in pilot studies). It may not always be necessary for dofetilide subtraction to be performed on the data, but we applied this method nonetheless to generate a gold-standard dataset.

4.5 Deriving I–V Curves and Time constant-V Curves

To derive time constant-voltage relationships from experimental data and simulated data traces, we used the Levenberg-Marquardt algorithm with a tolerance of 10^{-6} within Clampfit v10.5. To derive the instantaneous inactivation time constant curves shown in Figure 4 (inactivation column, row D) we fitted a single a single exponential to the current responses during the 150 ms V_{step}, as defined in the inactivation protocol (Pr4) description above.

To produce the deactivation and recovery from inactivation rate time constant–voltage relationship for the experimental data traces, we fitted a triple exponential through the experimental data trace from the deactivation protocol (Pr 5). The section of the data used for fitting is the current in response to the 6 second V_{step}. Both this region of experimental data used for fitting and that for the instantaneous inactivation time constant described above are highlighted in row B of Figure 4. The fastest time constant from the triple exponential fit to each test step corresponded to the recovery from inactivation time constant. We then used the weights of the remaining two time constants from each triple exponential fit to produce a single weighted time constant for deactivation[39]. To derive the deactivation and recovery from inactivation time constants from simulated data we fitted a double exponential through the current in response to the 6 second V_{step} section of the deactivation protocol. Again, we used the faster time constant as the recovery from inactivation time constant and the slower time constant as that for deactivation.

To produce the peak current-voltage relationship for the steady state activation protocol for the simulated data traces we wrote MatLab code to identify the peak current in the region between 5.6292 and 5.7292 seconds on each sweep of the protocol, which corresponds to the current response just after the 5 second V_{step} when the voltage is stepped to -40 mV. We then normalized the peak current data to the maximum overall peak identified in this region to produce the current-voltage relationship curve. For the simulated data we wrote a MatLab script (for additional details see Supplementary Code) to identify the peak-current voltage relationship for this protocol but for the experimental traces we verified these peak points manually to avoid incorrect peaks being identified due to noise or capacitive effects. We also identified the peak currents in the currents evoked by the activation kinetics protocols manually for the same reason. In the activation kinetics protocol we identified the peak currents during the V_{step} for each interval of T_{step} duration.

4.6 Mathematical Model Equations

The system of ordinary differential equations underlying the mathematical model structure shown in Figure 3B is as follows;

$$\frac{\mathrm{d}C}{\mathrm{d}t} = -(k_1 + k_3)C + k_2 O + k_4 IC, \tag{3}$$

$$\frac{\mathrm{d}O}{\mathrm{d}t} = -(k_2 + k_3)O + k_1 C + k_4 IO, \tag{4}$$

$$\frac{\mathrm{d}IO}{\mathrm{d}t} = -(k_2 + k_4)IO + k_3 O + k_1 IC, \tag{5}$$

where

$$IC = 1 - C - O - IO. \tag{6}$$

The eight parameters P_1 to P_8 determine the rates k_1 to k_4 as shown in Figure 3B. The current, I_{Kr}, is modeled with a standard Ohmic expression:

$$I_{\mathrm{Kr}} = G_{\mathrm{Kr}} O \left(V - E_K\right), \tag{7}$$

where G_{Kr} is the maximal conductance, E_K is the Nernst potential for potassium ions, and O is the open probability, given by the solution to the system of equations above. E_K is calculated from the ratio of ion concentrations on each side of the cell membrane:

$$E_K = \frac{RT}{zF}\left(\frac{[K]_{\mathrm{out}}}{[K]_{\mathrm{in}}}\right). \tag{8}$$

where R is the ideal gas constant, T is the temperature, F is the Faraday constant, z is the valency of the ions (in this case 1), and $[K]$ represents the concentration of potassium ions. Note that this expression has a temperature dependence, and the temperature of the bath was recorded for each cell and used in relevant simulations.

All simulations were performed in MatLab. Mex functions were used to define and simulate each hERG channel model with CVODE[40] used to solve the systems of differential equations, with both absolute and relative tolerances set to 10^{-8}. Code is available to download as described at the end of the main manuscript.

4.7 Parameter Inference

Parameters were estimated using a Bayesian Inference scheme similar to that described in Johnstone *et al.*[41]. Here we outline the likelihood function formulation. In Supplementary Material A2 we give details of how this likelihood is used to generate a posterior distribution for the parameter set.

4.7.1 Likelihood formulation

For an observed experimental recording which we will denote $\mathbf{y}$, we can infer the probability of different combinations of model parameters θ. Bayes' rule underpins this approach which is expressed as

$$P(\theta|\mathbf{y}) = \frac{P(\mathbf{y}|\theta)P(\theta)}{P(\mathbf{y})} \tag{9}$$

$P(\theta|\mathbf{y})$ is a probability density that encodes our belief that the parameters of the model are in a neighborhood of θ after observing the experimental data $\mathbf{y}$, and is termed the *posterior probability density*. $P(\mathbf{y}|\theta)$ is the probability density that corresponds to the probabilistic generation of the

experimental data $\mathbf{y}$ given a model parameterized with parameters θ. $P(\theta)$ encapsulates our beliefs about θ before observing any experimental data and is termed the *prior distribution* (details of the prior that we used are in Supplementary Material A2.2). $P(\mathbf{y})$ is a normalizing term which is the integral of all possible probabilities $P(\mathbf{y}|\theta)$ and ensures that the posterior density $P(\theta|\mathbf{y})$ integrates to 1. In practice this normalizing term is calculated by

$$P(\mathbf{y}) = \int P(\mathbf{y}|\theta)P(\theta)\mathrm{d}\theta. \tag{10}$$

A Bayesian inference approach to parameter estimation combines beliefs about the parameters in the prior distribution $P(\theta)$ with the *likelihood* $P(\mathbf{y}|\theta)$ to determine the posterior probability distribution $P(\theta|\mathbf{y})$.

We define the likelihood

$$L(\theta|\mathbf{y}) = P(\mathbf{y}|\theta) \tag{11}$$

to insist on the fact that we consider it as a function of θ, with $\mathbf{y}$ kept fixed at the observation values. Bayes' rule (in Equation (9)) can be rewritten in terms of likelihood as

$$P(\theta|\mathbf{y}) \propto P(\theta)L(\theta|\mathbf{y}). \tag{12}$$

When the prior distribution is assumed to be uniform (as it is in this study), we can make inferences based on just the likelihood, as the prior $P(\theta)$ is either constant or zero. If a proposed parameter is outside our chosen prior then likelihood is 0 and we simply record that this parameter set has a likelihood of 0 and propose another parameter set.

We assume that the errors at each time point are independent and so the conditional probability density of observing the whole experimental trace from time sample 0 to time sample T given the model parameter set θ is

$$L(\theta|\mathbf{y}) = \prod_{t=0}^{T} P(y_t|\theta). \tag{13}$$

We assume that the experimental noise is independently and normally distributed with a mean of zero and variance of σ^2. The likelihood is then expressed as

$$L(\theta|\mathbf{y}) = \prod_{t=0}^{T} \mathcal{N}(y_t|f_t(\theta), \sigma^2) = \prod_{t=0}^{T} \frac{1}{\sqrt{2\pi\sigma^2}} \exp\left(-\frac{(y_t - f_t(\theta))^2}{2\sigma^2}\right). \tag{14}$$

In our case $f_t(\theta)$ is the predicted current at each time point given the parameters, this is given by equation (7) after solving the model system (equations (3)–(6)). Calculating equation (14) requires the evaluation of the product of many numbers less than 1, so it is more numerically convenient to calculate the *log-likelihood* instead. As our aim is to identify parameter sets θ which maximize the likelihood in equation (14), maximizing the likelihood is equivalent to maximizing the log-likelihood:

$$\log\left(L(\theta|\mathbf{y})\right) = -\frac{1}{2}\sum_{t-0}^{T} \log(2\pi\sigma^2) - \frac{1}{2}\sum_{t=0}^{T} \frac{(y_t - f_t(\theta))^2}{\sigma_2}. \tag{15}$$

In practice, the sums over time in equation (15) are formulated so that we exclude time points from regions where the data are affected by capacitive spikes. To be precise, we exclude 10 ms intervals following step-changes in the imposed voltage clamp. In the sine wave protocol (Pr7) these step-changes occur at 0.25 seconds, 0.3 seconds, 0.5 seconds, 1.5 seconds, 2 seconds, 3 seconds, 6.5 seconds and 7 seconds (spikes are seen in experimental recordings at these times in Figure 2).

4.8 Note on Normalization

Where existing literature model simulations were plotted alongside experimental traces, or one experimental trace was compared with another, we first had to normalize to account for differences in conductance values and allow clearer comparison. This was achieved by selecting a scaling factor for the conductance value for each model simulation (or experimental trace) that minimized the square difference between each trace and a reference experimental trace.

For literature models the reference trace was the experimental current from the action potential clamp Pr6. Note this provides a best-case fit for Pr6 all of the models, removing the possibility that some models open 'half as much' because they have 'twice the conductance'. For the new model, no scaling was applied and conductance was directly fitted to the experimental current from the sine wave protocol (along with other parameters).

References

38. Cooper, J., Scharm, M. & Mirams, G. R. The cardiac electrophysiology web lab. *Biophysical journal* **110,** 292–300 (2016).

39. Lacroix, J. J., Labro, A. J. & Bezanilla, F. Properties of deactivation gating currents in Shaker channels. *Biophysical journal* **100,** L28–L30 (2011).

40. Hindmarsh, A. *et al.* SUNDIALS: Suite of nonlinear and differential/algebraic equation solvers. *ACM Trans. Math. Software (TOMS)* **31,** 363–396 (2005).

41. Johnstone, R. H. *et al.* Uncertainty and variability in models of the cardiac action potential: Can we build trustworthy models? *Journal of Molecular and Cellular Cardiology* **96,** 49–62 (2016).